BRIGHT LESIONS DETECTION IN RETINAL IMAGES

USING VARYING BOX SIZES

By

Sana Alam

A thesis submitted to the faculty of Electrical Engineering Department,
Military College of Signals, National University of Sciences and Technology,
Islamabad, Pakistan, in partial fulfillment of the requirements for the degree of MS in
Electrical Engineering

December 2015

CERTIFICATE

It is to certify that final copy of thesis has been evaluated by me, found as per specific format and error free.

Dated: _____

_____

(Lt Col Abdul Ghafoor, PhD)

ABSTRACT

Image processing has gained lot of importance over the last few years. Its applications are used in almost all the fields especially medical field. The development of automated techniques for detection of diabetic eye diseases has become a reality with the exponential evolution of information processing system and the emergence of economical ophthalmic imaging devices. Several automated techniques are being designed and used for practical applications all over the world.

Digital retinal imaging uses high-resolution imaging system to take pictures of the inside of eye. This helps the doctors assess and manage the health of retina. Retinal imaging provides opportunity for the diagnosis of several medical pathologies. A particular type of pathology which occurs due to diabetic retinopathy is bright lesions. The manual analysis of retinal images is time-consuming and expensive. The automation of certain processing steps is thus important and facilitates the subsequent decisions by specialists to provide a basis for early diagnosis steps of specific diseases. The automatic segmentation of the vessel tree is an important processing step which facilitates subsequent automatic processes that contribute to such diagnosis. This can help to point out the area of disease. This work propose an automatic/semi-automatic technique to distinguish non-disease images and disease images containing bright lesions.

The proposed work will contribute to the development of a system which can be used in hospitals to pre diagnose the cases and refer the relevant cases to the ophthalmologist for attention. The research can pre-diagnose the bright lesion cases in patients and automate the disease detection.

DEDICATION

This thesis is dedicated to

MY FAMILY, FRIENDS AND TEACHERS

for their love, endless support and encouragement

ACKNOWLEDGEMENTS

I thank Allah Almighty for bestowing me with endless blessings, the opportunity and the strength to complete my work. I am grateful to my parents, siblings and husband for the endless support, prayers and bearing till the completion of the project. Thank you for being my moral support.

A lot of credit goes to my supervisor Lt. Col Dr. Abdul Ghafoor and co-supervisor Dr. Mohsin Riaz, I thank them for their guidance, time, patience and support.

Very special thanks to my friends for giving me moral support.

Lastly I extend earnest gratitude to MCS, NUST for providing a channel to present my work.

TABLE OF CONTENTS

LIST OF FIGURES

ACRONYMS

Bar-Combination Of Shifted Filter Responses	B-COSFIRE
Diabetic Retinopathy	DR
Region of Interest	ROI
Contrast Limited Adaptive Histogram Equalization	CLAHE
Cotton Wool Spot	CWS
Hard Exudate	HE
Diabetic retinopathy	DR
Micro Aneurysm	MA
Hemorrhage	H
Red Green Blue	RGB
Hue Saturation Value	HSV

Chapter 1

INTRODUCTION

1.1 Background

Digital retinal imaging uses high-resolution imaging system to take pictures of the inside of eye [1-5]. It helps the doctors assess and manage the health of retina and for diagnosing several medical pathologies. The manual analysis of retinal images is time consuming and expensive [6]. The automation of certain processing steps is thus important and facilitates the subsequent decisions made by specialist it provides a basis for early diagnosis of specific diseases. Diabetic Retinopathy (DR) is a progressive ailment which can cause blindness [7], it is one of the most common reasons of blindness around the world. Diabetes is the most common disease that causes DR, it causes swelling and leakage or the creation of new blood vascular network in a fundus. Failure in early detection of these changes can result in blindness as the leakage can get deposited nearby the fovea or Optic Disc (OD) distressing the vital vision of the eye [8]. However the risk of vision loss and blindness may be reduced if it is detected early, many image processing techniques can be used to identify such lesions in retinal images [9] [10].

DR is classified into bright and dark lesions. Bright lesions are further classified into Cotton Wool Spot (CWS) and Hard Exudate (HE) and dark lesions into Micro Aneurysm (MA) and Hemorrhage (H) [11]. HE are yellowish small-large irregular sharp bright lesion and CWS are whitish small medium oval shaped blur. CWS shows severe case of vascular deficiency to an area of retina [12]. Buildup of axoplasmic material within the nerve fiber layer causes damage to nerve fibers. The disease categorization and classification of fundus images is a repetitive (time consuming) process that require the attention of an ophthalmologist and consequently increases the work load significantly. Moreover many of the fundus images do not contain any pathology. Therefore an automatic disease categorization and classification is desirable [13].

1.2 Problem Statement and Motivation

The processes of categorizing the eye fundus images are time consuming and repetitive, requiring the time and attention of an ophthalmologist. Many of the fundus images do not contain any pathologies related to the disease. Also an ophthalmologist work load significantly increases as the development of the disease needs to be monitored regularly. By automating the system, patients can be grouped that require the attention of ophthalmologist and be sent for further examination, in this way a lot of the time can be saved as the ophthalmologist can move directly to disease cases instead of going through each and every fundus image.

1.3 Objectives

The objective of our proposed scheme is to develop an automatic/semi-automatic technique to distinguish non-disease images and disease images containing bright lesions. Furthermore the type of bright lesion present is identified and classified into CWS or HE.

1.4 Contributions

Main contributions of this research are

- Development of an automated/semi-automated system which can be used in hospitals to pre diagnose the cases and move the relevant cases to the ophthalmologist attention.
- Correct detection and classification of disease as CWS or HE.

1.5 Advantages

The research will prove to be quite useful in many perspectives, such as:

- Help doctors in pre diagnosing the bright lesion cases in patients.
- The manual work of retinal analysis could be very time-consuming and is influenced by human subjectivity so the automated disease detection can preprocess the relevant cases.

The proposed image processing techniques can be used for detection of disease in medical field. Image processing has gained lot of importance over the last few years. Its applications are used in almost all the fields especially medical field. The development of automated

techniques for detection of diabetic eye diseases has become a reality with the exponential evolution of information processing system and the emergence of economical ophthalmic imaging devices. Several automated techniques are being designed and used for practical applications all over the world. The proposed work will contribute to the development of a system which can be used in hospitals to pre diagnose the cases and move the relevant cases to the ophthalmologist attention.

1.6 Thesis Outline

This thesis is divided into six chapters:

Chapter 1: This chapter is the basic introduction of the topic, problem statement, scope and objective.

Chapter 2: This chapter contains literature review, including B-COSFIRE which is used to segment the vessels from the fovea, background and Optic Disc. This chapter gives the basic understanding of vessel segmentation.

Chapter 3: This chapter explains the extraction of disease area, narrowing down the disease area, classifying the disease as CWS or HE.

Chapter 4: This chapter is about the experimental and simulation results carried out.

Chapter 5: Last chapter is about conclusion and future work.

Chapter 2

LITERATURE REVIEW

2.1 Background

Various techniques exist in literature for segmenting of vessels and classification of disease [16-42]. The contrast, between retinal blood vessel and surrounding background fovea, can be used for retinal vascular segmentation. It is piecewise linear, can be exemplified by sequence of connected small lines all originating from the optic disc [14]. Four main techniques are used to segment the vessel network form retinal images are matched filters, vessel tracking, neural networks and morphological processing [15]. Furthermore segmentation of blood vessels is of two types supervised [16-30] or unsupervised [31-38]. Supervised methods trains a classifier using pixel-wise feature vectors to distinguish between vessel and non-vessel pixels whereas unsupervised method implement any rule-based technique or thresholds filter responses.

The supervised works in [16-30] use initial points to track vessels and the vascular tree is attained by following the vessel center lines. Some of these works [20-23] use priori information, mathematical morphology, curvature analysis and linear filtering to distinguish between background and vessels. However these works are time inefficient. The works in [24-26] profile the vessels using matched filters however these works over detect the blood vessels due to edges of other bright objects (like optic disk). Better matched filter parameters were proposed in [27] however it is an exhaustive search optimization procedure. In [28] active contour model is used for segmentation however it fails to properly identify overlapping or closely parallel vessels. Multiscale analysis is used in [29] to segment vessels by using width, size and orientation information however it detects more blobs from background particularly in those images with strong pathologies. Multiconcavity model is used in [30] however it is time inefficient.

Out of unsupervised works [31-38], multiscale analysis of Gabor wavelets along with Bayesian classifier is used in [31] however it detects false noise and other artifacts. Rotation-

invariant line operator in combination with a Support Vector Machine (SVM) is introduced in [32] however it does not segment the degraded contrast or thinnest vessels properly. In [33] gray-level and moment invariants-based features are used in neural network for pixel classification, however the results are subjective. Classification scheme based on a collaboration of boosted and bagged decision trees is used in [34]. Combination of Receptive Fields computational model of a simple cell in visual cortex is used in [35] and its implementation called Combination of Shifted Filter Responses (COSFIRE) (discussed in [36], [37]) detects vascular bifurcations in retinal fundus images. In [38] a new filter B-COSFIRE, where B stands for bar (a generalization for representing a vessel), for vessel delineation performs automatic segmentation of blood vessels in retinal fundus images.

To categorize different lesion types such as cottonwood spot, exudates [39-40] there are a number of classification method. Phillips inspected [41-42] for exudates detection and identification. In [43] a multiscale principal curve projection and tracing algorithm is proposed for diagnosis and analysis of disease, however it lacks branches and bifurcation points. For detecting and characterizing target lesions [44] presents a general framework with k-NN classifier however the proposed filter framework with other classifiers may not be optimal. In [45] the blood vessels are detected by graph tracer, the crossover detection technique is used to identify vessel crossings. An algorithm for automatic detection of optic disc and blood vessel from blue plane of the image in presented in [46], this detection scheme constitutes of edge detection, binary thresholding and morphological operation, however the works in [45,46] need to be assessed on other databases.

The proposed scheme prescreens the fundus of the patient, categorizes as DR or not, and selects the fundus for formal screening. The type of bright lesion is identified and classified into CWS or EX. The proposed disease detection scheme is simple and it can lower the burden on the hospitals for manual screening by providing an automated/semi-automated system.

2.2 B-COSFIRE Filter (For Vessel Segmentation)

COSFIRE filter is used in interested point detection and pattern recognition, B-COSFIRE accomplishes orientation selectivity. RGB (red, green and blue) color images merges all three channels to represent an image [47]. From [29-31, 48] we gather that the green channel

delivers finest contrast between blood vessels and the background. Conversely, blue channel displays a small dynamic range and red channel displays a low contrast between the blood vessels and the background. In [21] evaluation of different color representations and their performances is discussed; between a-component of Lab color space, luminance component of National Television Systems Committee color space and green component of RGB color spaces. It concludes that in general the maximum contrast between vessels and background is shown in the green channel of the RGB color space.

To avoid incorrect detection of lines around the border of the FOV in a retinal image, the border is dilated by an iterative system. In the opening iteration all the pixels on the edge of the mask are considered, these pixels are substituted by the mean value of its 8-neighbours that are inside the region of interest (ROI). ROI radii increases by one pixel after each iteration. This process is reiterated approximately 50 times to make sure that no false detection happens. CLAHE is contrast-limited adaptive histogram equalization [49], it is generally a pre-processing step used while analyzing retinal images ([50], [51]). CLAHE improves the local contrast by eluding the over-amplification of noise present in comparatively homogeneous regions.

A vertical bar is used to configure B-COSFIRE filter. Center-on DoG(Difference of Guassian) filters gives us high response to intensity change in the input image, this is used as an input to B-COSFIRE filter. Basically, a center-on DoG filter with a particular ρ is applied to the sample input vertical bar. The result response is taken in general no. of concentric circles around the center point.

$$c_\sigma = |I \star DoG_\sigma| \tag{2.1}$$

where I is intensity value and $|.|^+$ shows half wave rectification.

Dominant intensity variation I around the circle is determined by the maximum response along the circle as shown in figure 2.1. Every I can be described by three parameters, σ, ρ and ϕ. ρ and ϕ gives polar coordinates, whereas σ represents the standard deviation.

$$S = \{(\sigma, \phi, \rho)|i = 1, \ldots, n\} \tag{2.2}$$

is a set of 3-tuples, here n stands for the number of considered DoG responses.

A B-COSFIRE filter output is the weighted geometric mean of the responses of the con-

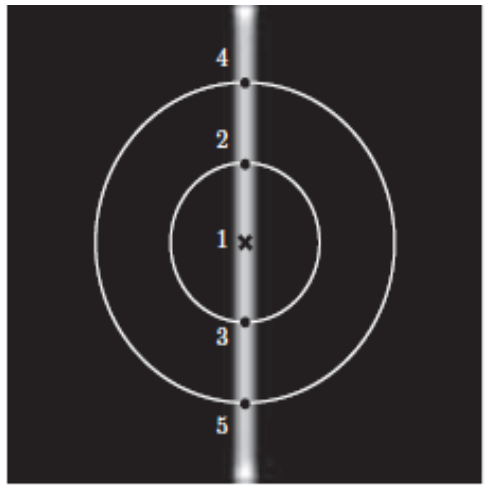

(a) Vertical bar used for configuration and the dominant intensity variation illustrated in circles around it

Figure 2.1

cerned DoG filters. To allow some lenience in the position of selective points, we blur the responses. First the coefficients of gaussian function $G_{\acute{\sigma}}(\acute{x}, \acute{y})$ are multiplied by the responses of the DoG filter, this constitutes the weighting. Blurring can be achieved by applying the maximum weighted threshold response of DoG filter. Weight is calculated by multiplying responses of DoG filter by the coefficients of a Gaussian function. After blurring each DoG response is shifted by ρ_i in the reverse direction of ϕ_i so that they meet at the support center of the B-COSFIRE filter. Output of a B-COSFIRE filter is the weighted geometric mean of all the blurred and shifted DoG responses that correspond to the tuples in the set S:

$$r_s(x,y) = |(\prod_{i=1}^{|S|}(s_{\sigma_i,\rho_i,\phi_i}(x,y))^{1/\sum_{i=1}^{|S|}\omega_i})| \tag{2.3}$$

where

$$\omega_i = \exp^{-\frac{\rho_i^2}{2\sigma^2}}, \hat{\sigma} = \frac{1}{3}\max_{i\epsilon\{1...|S|\}}\{\rho_i\} \tag{2.4}$$

This is an AND-type function i-e the filter attains a result when the response is greater than zero. Rotation invariance can be achieved by presenting a rotated bar or by changing the polar coordinates in S set to accommodate the rotated angle, consequently the output computation is very efficient. In theory the output AND function does not attain a response at vessel ending. However, in practical application the noisy background of the retinal images cause a response at vessel ends. To resolve this another filter is configured, in which the prototype is bar endings instead of whole bar. To distinguish between these filters they are

named symmetric B-COSFIRE filter and asymmetric B-COSFIRE filter respectively.

Summary:

In this chapter, existing B-COSFIRE Filter is discussed with detailed description. The pre-processing on the retinal image and extraction of vessels from background, fovea and OD is discussed.In the next chapter, efficient disease detection is discussed.

Chapter 3

PATCH EXTRACTION AND DISEASE DETECTION

3.1 Overview

The segmented binary image obtained by applying B-COSFIRE filter is shown in fig 3.1(a). This image contains no disease. Fig 3.1(b) shows the segmentation of a retinal image containing bright lesions. During the segmentation process the bright lesion get segmented as numerous small vessel endings. This can be used to detect the location of the area in which the disease is present. Once we narrow down the correct area of the disease, the type of bright lesion present (CWS or HE) can be detected by using RGB and HSV histograms in their respective color spaces.

3.2 Proposed Methodology

Let Z be the input image having dimensions $X \times Y$, represented in RGB color space.

$$R \xleftarrow{\text{B-COSFIRE}} \Big(Z, f_1, f_2, h_1, h_2\Big) \tag{3.1}$$

where f_1 and f_2 are is symmetric and asymmetric filters, h_1 threshold parameter used to suppress the input filters responses and h_2 is the threshold parameter used to select the channels of input filters. Applying imerode and imclose to R removes redundant small vessels, thus improving the image quality as shown in figure 3.2(a). Imerode is used to eradicates pixels whereas imclose performs dilation which is then followed by erosion. Dilation can be explained as increasing the pixel at the edge of an object in any image while erosion removes the pixels from the objects edge. Applying these functions in the code removes redundant small vessels/dots, thus improving the image quality.

$$R_e \quad \xleftarrow{\text{imerode/imclose}} \quad R \tag{3.2}$$

Let P_i be the i^{th} patch of R_e, which is divided into square blocks of equal sizes as shown in figure 3.2(b). The number of patches is the same across x-axis and y-axis of the image also each patch is uniform pixel-wise in length and width. The normalized number of vessels

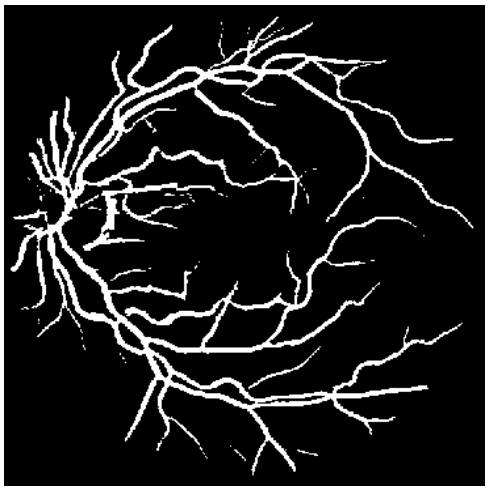

(a) Retinal image after B-COSFIRE processing containing no disease

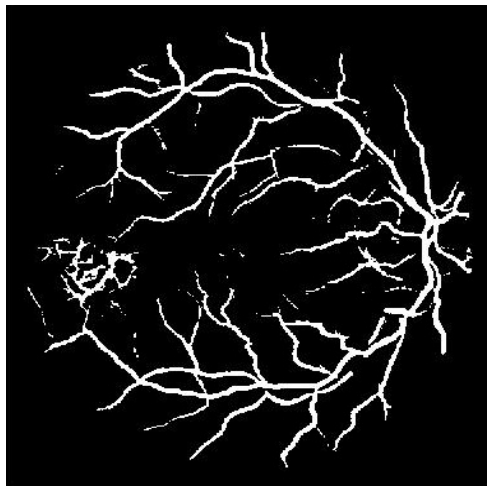

(b) Retinal image after B-COSFIRE processing containing disease

Figure 3.1

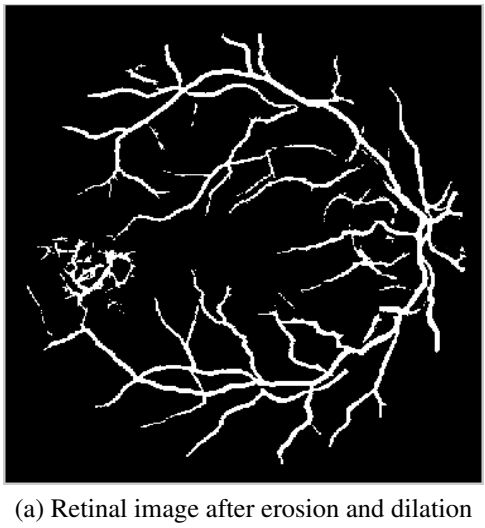

(a) Retinal image after erosion and dilation

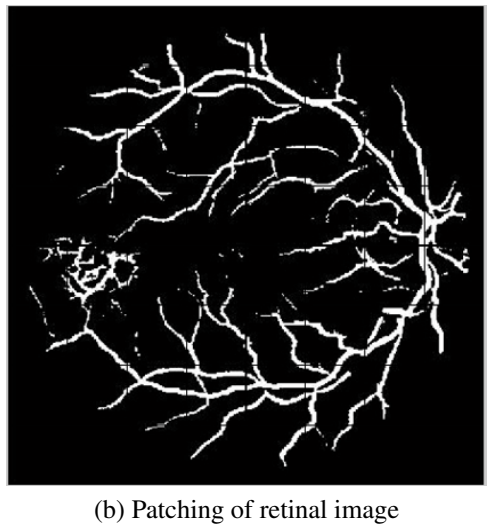

(b) Patching of retinal image

Figure 3.2

in each patch is given as :

$$V_i = \frac{\sum_k P_i(k)}{X_i Y_i} \tag{3.3}$$

where k represents non-zero values in P_i and $X_i \times Y_i$ is the size of i^{th} patch. The disease box is extracted as,

$$\tilde{V} = \max_i(V_i) \tag{3.4}$$

The box $\tilde{V}$ is then translated and scaled around the center to obtain different boxes $\tilde{V}^{(j)}$. i-e the image is moved in all directions in different coordinate combinations around the original coordinate points. The box $\dot{V}$ with maximum normalized number of edges is selected. Figure 3.3 shows the how disease is detected in retinal images and narrowed down to the correct box.

By taking the histogram of the narrowed down disease box, we can determine the disease type. In photography and image processing a color histogram represents the distribution of colors in an image, it illustrate the number of pixels of each color (all possible colors in a fixed list of color ranges) that span the images color space. There are different color spaces and a color histogram can be built for any color space, frequently used color spaces include RGB color space and HSV color space. RGB color space includes the three primary colors red, green and blue and it handles all the secondary colors made up by these basic colors components in an image. RGB color space has a cubic representation as shown in figure 3.4(a). HSV color space has a cylindrical geometry, it reorganize the geometry of RGB in order to be extra relevant and intuitive in comparison with the cubic representation commonly known as cartesian representation. In the cylindrical representation, hue is the angle around the central vertical axis, saturation is the distance from the axis, and value is the distance along the axis as shown in figure 3.4(b). An RGB histogram demonstrate the red, green and blue color and their contributions in the composition of an image whereas HSV histogram represents hue, saturation and intensity components of an image and the number of pixels representing each component.

Now let $\dot{Z}$ be the patch extracted from original image Z corresponding to $\dot{V}$ box, the

(a)

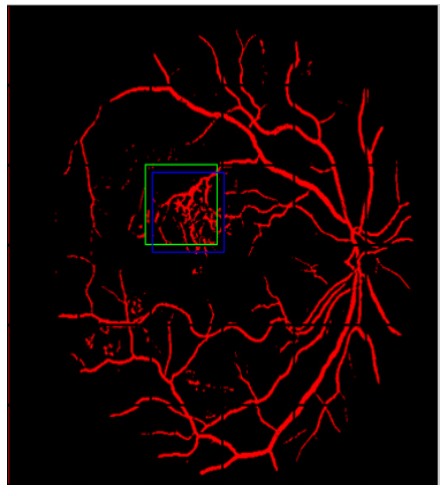

(b)

(c)

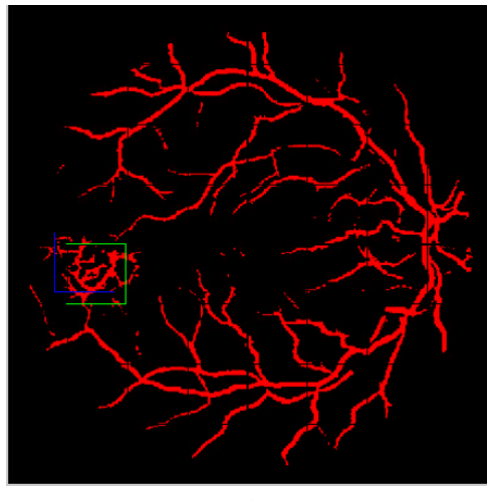

(d)

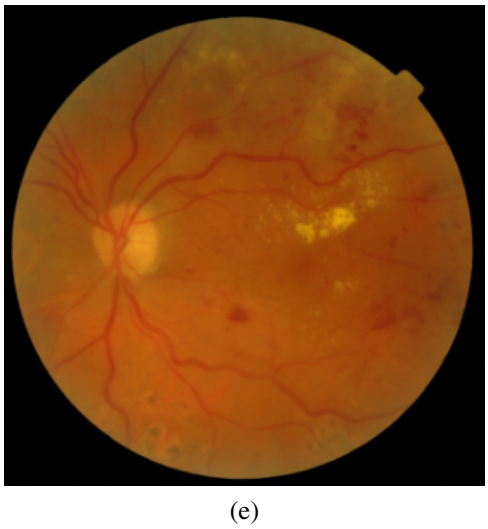

(e)

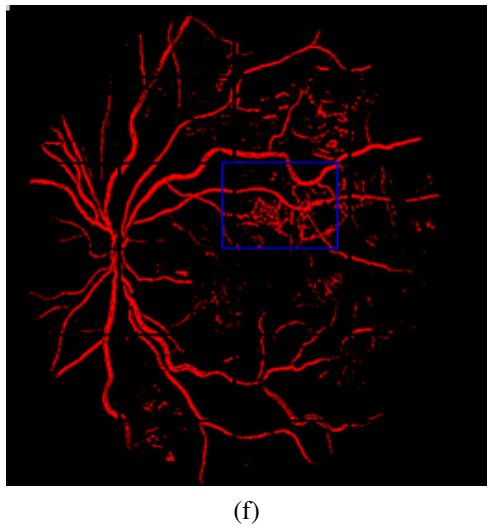

(f)

Figure 3.3: Retinal image disease detection (a),(c),(e) Retinal image containing disease (b),(d),(f) Disease is detected and narrowed down to the exact area

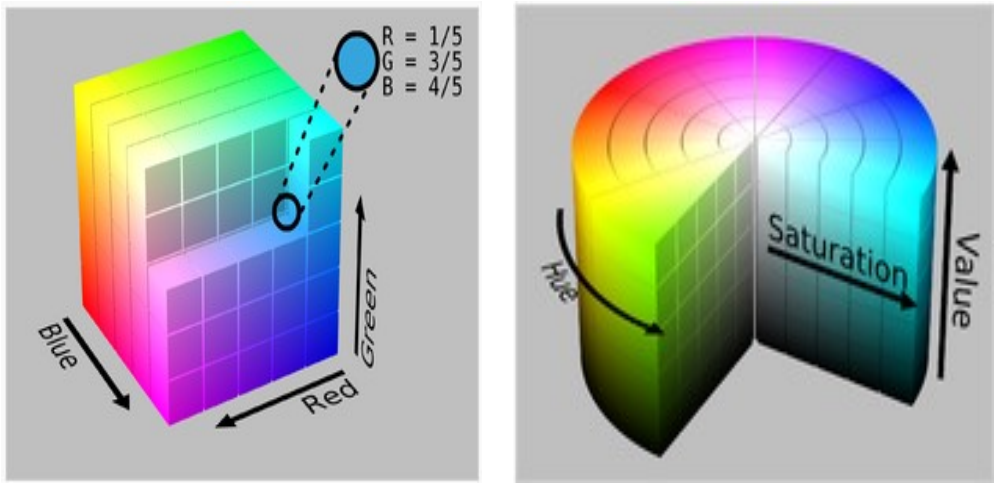

(a) (b)

Figure 3.4: (a) RGB color space (b)HSV color space

histogram of red component is

$$\psi_R \xleftarrow{\text{Histogram}} \dot{Z} \tag{3.5}$$

The $\dot{Z}$ is converted into HSV color space and the histogram of H component is

$$\psi_H \xleftarrow{\text{Histogram}} \dot{H} \tag{3.6}$$

For CWS the condition is

$$200 \leq \overline{\psi}_R \leq 250 \quad and \quad \overline{\psi}_H \geq 0.1 \tag{3.7}$$

For HE the condition is

$$100 \leq \overline{\psi}_R \leq 150 \quad and \quad \overline{\psi}_H \leq 0.1 \tag{3.8}$$

where $\overline{\psi}_R$ and $\overline{\psi}_H$ are mean values of ψ_R and ψ_H respectively.

If the value of histogram lies between 200 to 255 in red component of RGB histogram and more than 0.1 in hue component in HSV histogram, this indicates the disease present is CWS as shown in Fig 3.5 and Fig 3.7. If the value of histogram lies in-between 100 to 200 in red component of RGB histogram and less than 0.1 in hue component in HSV histogram this indicates the disease present is HE as shown in Fig 3.7 and Fig 3.8.

To further refine the results, the disease region is separated from the background using Color Names for Real-World[30]. For preprocessing the RGB color space is converted into

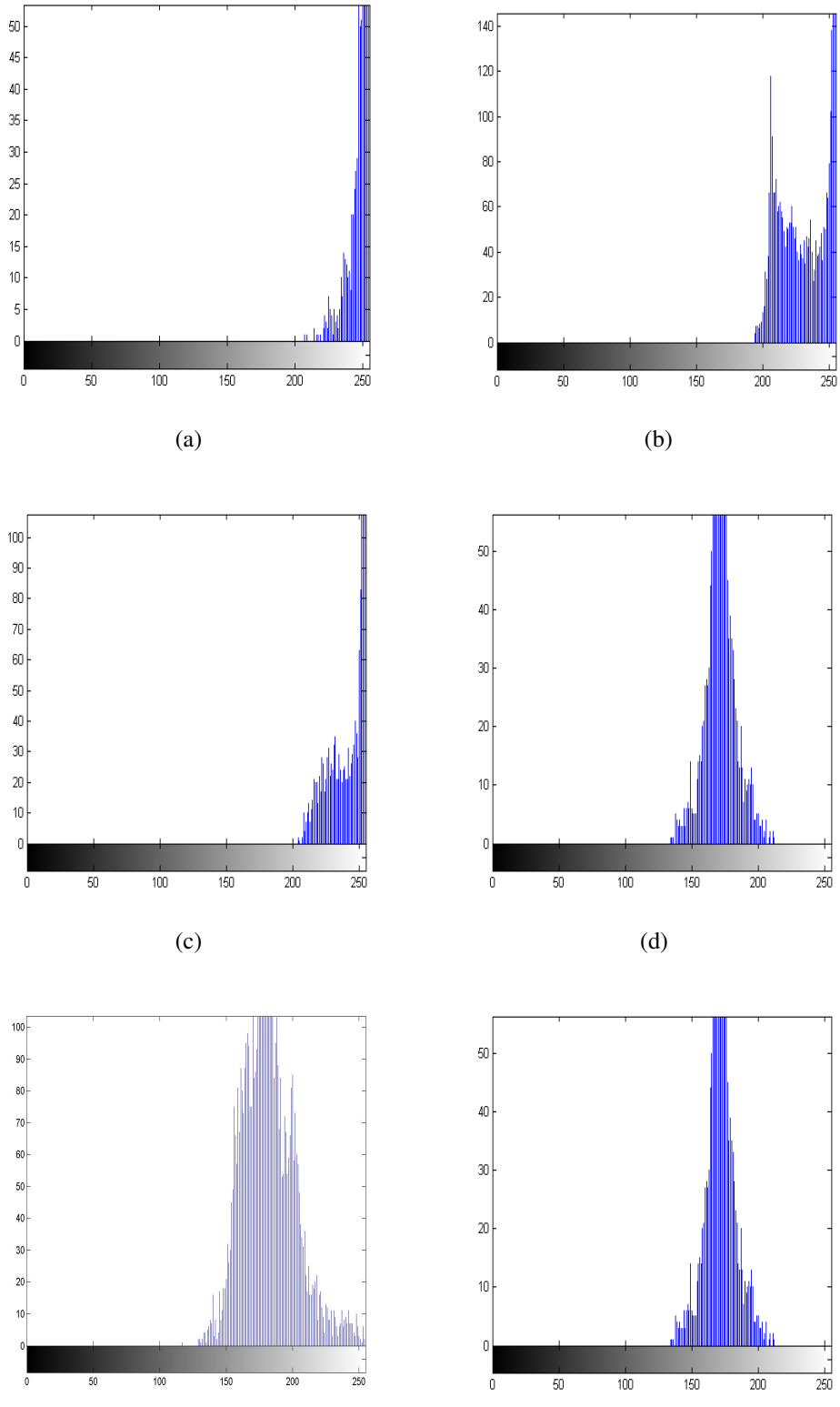

Figure 3.5: Histogram of red component for CWS are shown in part a, b and c and for HE disease in d, e and f.

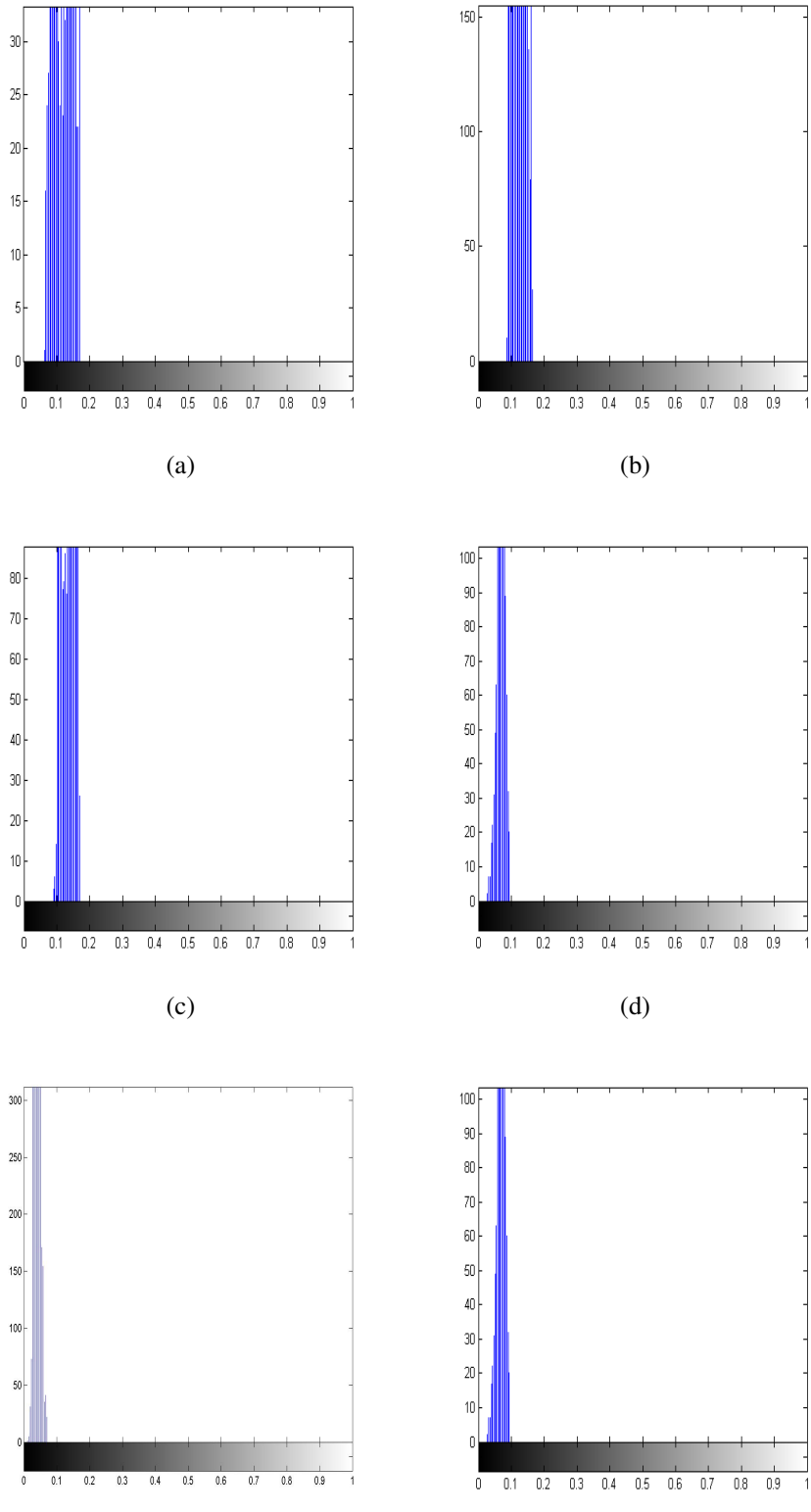

Figure 3.6: Histogram of hue component for CWS are shown in part a, b and c and for HE disease in d, e and f.

L*a*b color space. This color space includes all perceivable colors where L represents lightness and a, b represents color-opponent dimensions, based on nonlinear compressed coordinates. The most significant quality of this color space is its device independency, meaning the nature of the color origin or the displaying device specs do not interfere with its representation. It is a real number space with infinite possible combinations and representations of all the possible colors, however practically the space gets mapped onto a three-dimensional integer space where L, a, b values are within a pre-defined range.

$$\tilde{Z} \xleftarrow{\text{L*a*b color space}} \dot{Z} \tag{3.9}$$

Usually a collection of categorized color chips is used to learn color names, the labels are defined by well executed experimental setup, using humans as test subjects. However, between experimental setting and real world images, the defining and tagging of colors differs significantly. The adapted PLSA model given in the paper [30] as compared to the standard model, shows that in real world applications chip-based color naming lacks in comparison to color naming learned from real-world images. This technique is used to separate the disease from the background.

$$\overline{Z} \xleftarrow{\text{color attributes}} \tilde{Z} \tag{3.10}$$

This completely separates the disease and the background, giving us a clear boundary of the disease, from this we can determine the size and shape of the disease which also gives us visual confirmation of disease type. Once the disease is completely separated we take out the disease part only and take its RGB and HSV histograms. Now these are the exact histograms as they are free of the small background areas, which where present in the disease box extraction before. Figure 3.9 and 3.10 shows the results after applying this technique on the previously obtained results i-e the disease boxes.

When we take histogram of the disease box, if the value of histogram lies in-between 0 to 200 in RGB histogram and less than 0.1 in HSV histogram this indicates the disease present is HE and if the value of histogram lies between 200 to 255 in RGB histogram and more than 0.1 in HSV histogram, this indicates the disease present is CWS.

After applying color attributes, in the case CWS disease is present R component histogram

shrinks down to mean value of 250 and H component reduces to 0.15 as shown in figure 3.11 and 3.13 respectively. In case HE disease the R component of histogram spreads over 200 to 250 scale and H component has the peak value at 0.1 as shown in figure 3.12 and 3.14 respectively.

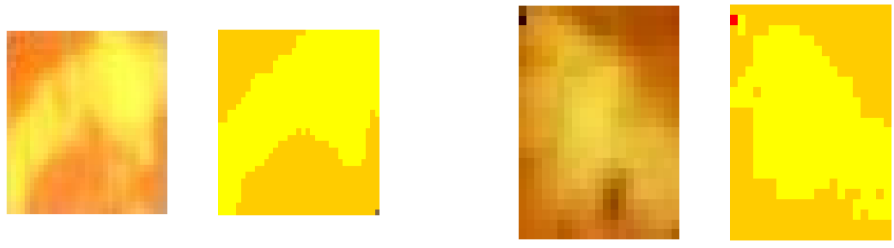

(a) (b)

(c) (d)

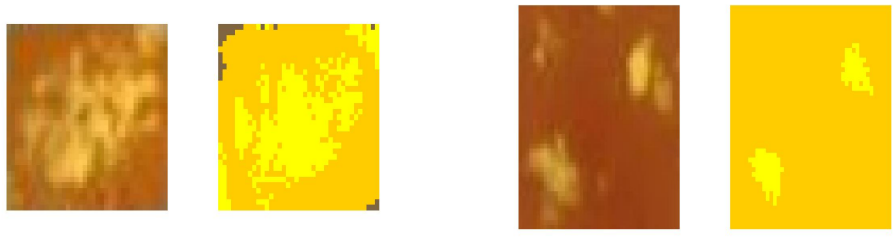

(e) (f)

Figure 3.7: CWS disease results after applying color attributes are shown in part a, b and c and HE disease results in part d, e and f.

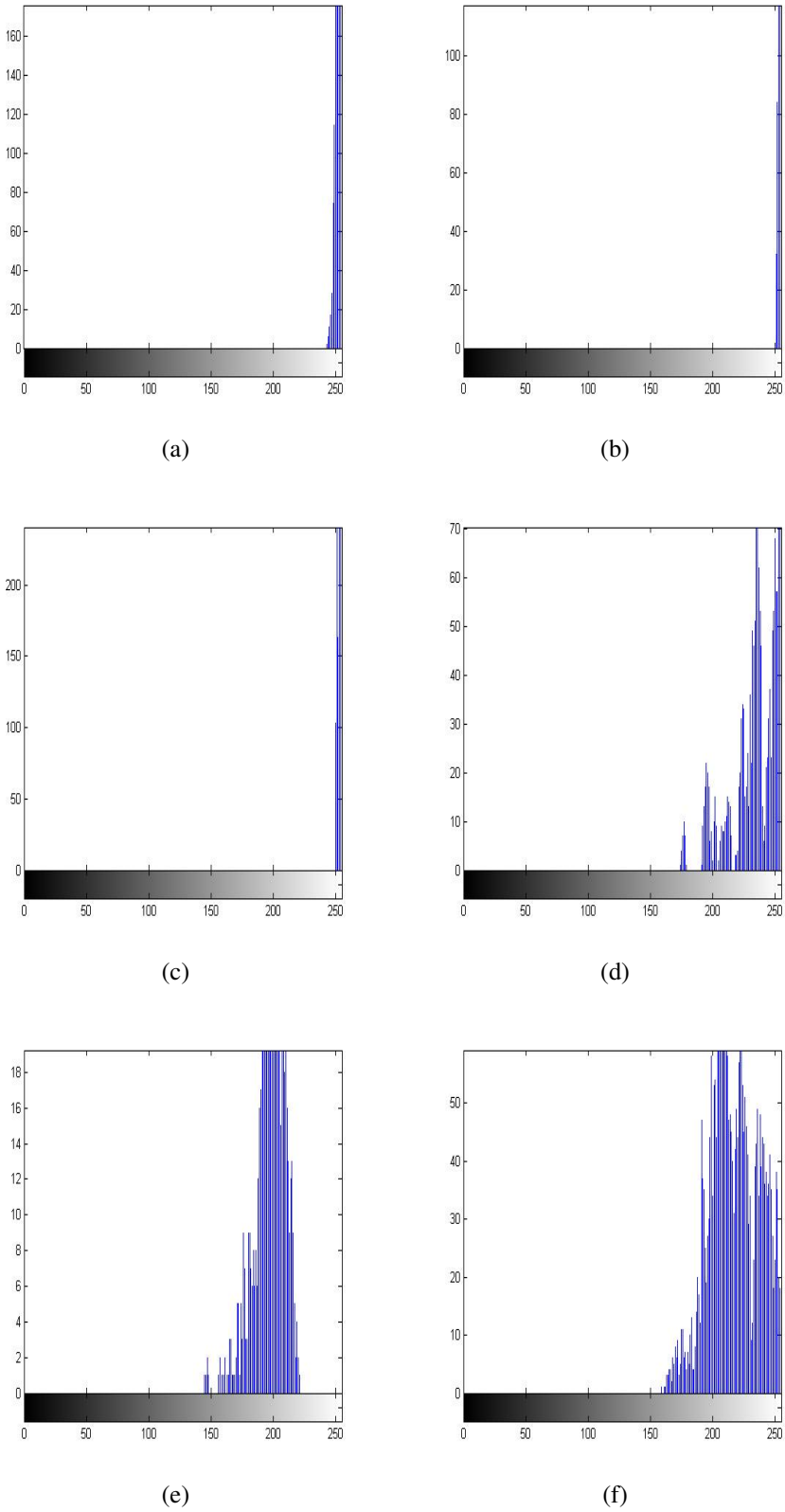

Figure 3.8: Histogram of red component for CWS disease after applying color attributes are shown in part a, b and c and for HE disease in d, e and f.

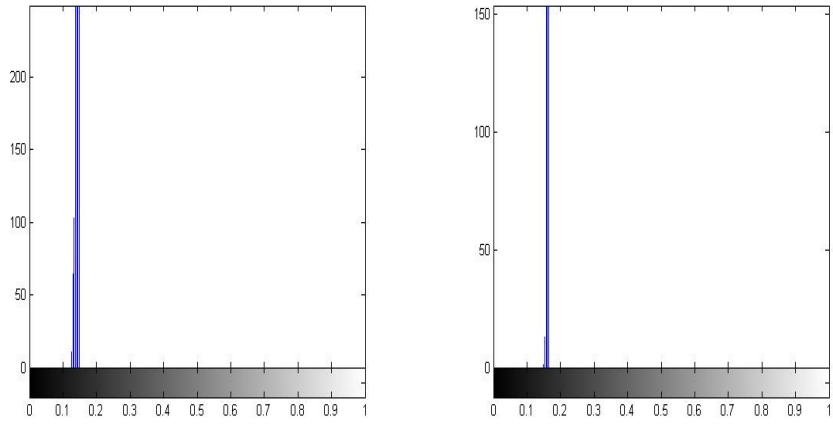

(a) (b)

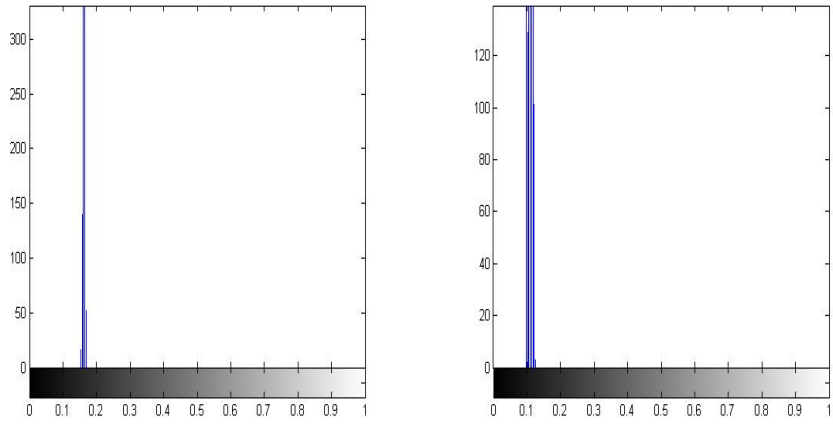

(c) (d)

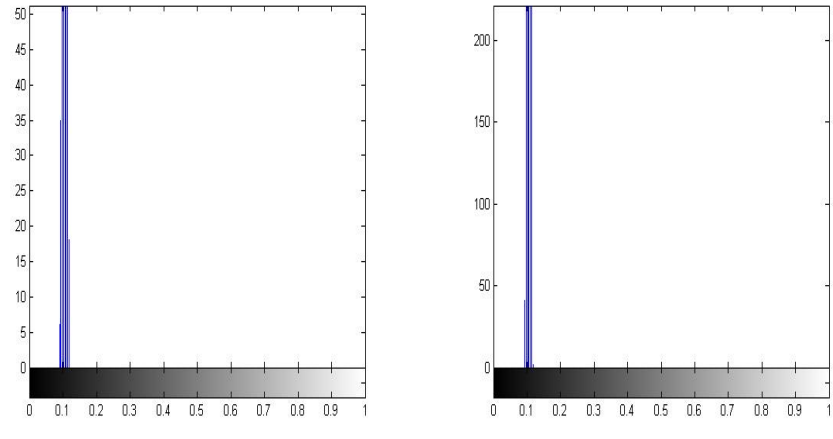

(e) (f)

Figure 3.9: Histogram of hue component for CWS disease after applying color attributes are shown in part a, b and c and for HE disease in d, e and f.

Chapter 4

RESULTS AND DISCUSSION

In this chapter the proposed methodology is explained elaborately with the help of an example. The system used in this experiment is a 64-bit operating system, x-64 based processor, having a RAM of 4.00 GB, intel core i5-4210U and CPU performing at 2.40GHz. The software used is MATLAB R2013-b 32-bit version. 32-bit version is used because it supports some of the functions used in the code which are not fully supported by 64-bit version causing changes in the results. The data sets used are DRIVE, STARE, $CHASE_DB1$ and Masidore Base 11-14 1nd 22-24. DRIVE database contains retinal images from a screening program from The Netherlands. 400 diabetic test subjects of age 25-90 were screened. 40 retinal images were selected abstractly, 33 of these show no signs of DR and 7 show presence of DR. These images are divided into training and test sets, both having 20 retinal images each.The Structured Analysis of the Retina (STARE) was initiated by Micheal Goldbaum. The data set contains 20 retinal images; 10 clear of any pathology and 10 having signs of pathologies. Two different observers have manually segmented the images. $CHASE_DB1$ database consists of 28 color retinal images from 14 patients participating in the program Child Heart And Health Study in England. This database is manually segmented by two observers. Messidor database contains 1200 retinal images, acquired by 3 ophthalmologic departments. These images are packaged in 3 sets, one by each department. Each set is further divided into 4 sub sets containing each 100 images in TIFF format. We have used Bases 11-14 and 21-24

4.1 Elucidation with Example

CASE:

Disease Type : HE

Database : Masidore, Base 24

Figure 4.1 shows first four steps i-e applying B-COSFIRE filter, erosion and dilation, followed by patching and disease detection. The first step after segmentation is patch extraction.

(a) Retinal image

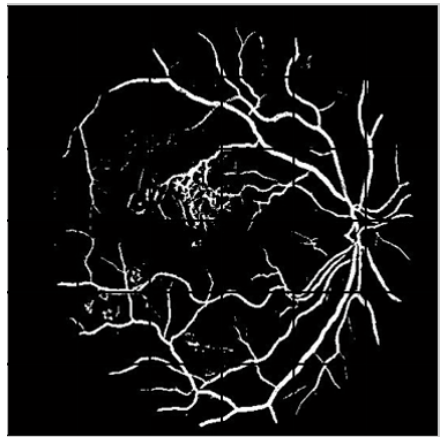

(b) Retinal image after B-COSFIRE processing and erosion

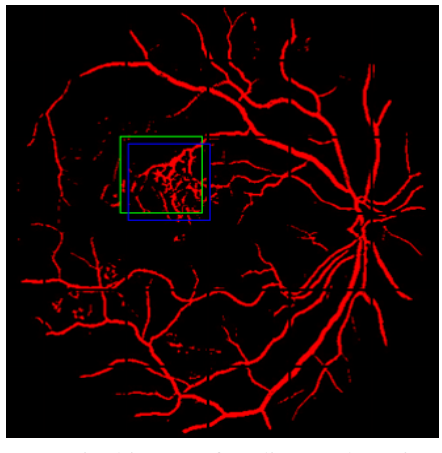

(c) Retinal image after disease detection

Figure 4.1

The segmented image is resized and divided into an a×a number of patches. Each patch is further contains b rows and b columns. Each patch is accessed and number of edges present in that particular patch is calculated. The patch containing the highest number of edges is then selected for further processing.

This retinal image is segmented in to an array of 6×6 patches, each patch further contains 60×60 pixels. Edges present in each patch is calculated while dividing the image into patches.

Patches =

Columns 1 through 7

304 302 1167 1519 604 244 461

Columns 8 through 14

1290 1759 2320 1831 759 527 2191

Columns 15 through 21

2671 2463 2599 1586 672 1976 1508

Columns 22 through 28

1212 2350 1480 489 2115 2361 2265

Columns 29 through 35

2653 865 531 862 2453 2231 1571

Column 36

484

Maximum edges present in a patch = 2671

The position of this patch is calculated by determining the starting row and column point of this patch.

Let

DBx	=	Disease Box
Ps	=	Patch Size
Rn	=	Row no. containing the disease box
Cn	=	Column no. containing the disease box
X1	=	Row starting point
X2	=	Row ending point
Y1	=	Column starting point
Y2	=	Column ending point
n	=	Represents different box locations and sizes
R	=	Ratio of edges over area
Output	=	Output image

After determining the location of disease patch, the row containing the disease box is calculated.

$$Rn = floor(DBx/(Ps/10)) \tag{4.1}$$

From this we can determine the starting and ending point of disease patch.

$$X1 = Rn * (Ps + 2) \tag{4.2}$$

$$X2 = Rn * (Ps + 2) + Ps + 2 \tag{4.3}$$

Similarly the starting and ending column points of the disease patch are also determined.

$$Cn = DBx(Rn * Ps/10) \tag{4.4}$$

$$Y1 = (Cn * Ps)(Ps) \tag{4.5}$$

$$Y2 = ((Cn * Ps)(Ps)) + (Ps + 2) \tag{4.6}$$

Now we have four sets of x, y coordinate points which frames the disease patch. By connecting these coordinate points the disease box is highlighted. This is a rough estimate of the area where the disease is present. To refine our search we translate and scale the disease box around the center to obtain different boxes. By moving each coordinate set by [-8,8] pixels in all direction (i-e sideways, upwards and downwards) and combinations we

cover a safe area over which disease can be present and determine the best boundaries for the patch containing the disease.

We then determine the ratio of edges over area of all these translated and scaled disease boxes.

$$R(n) = DBx(n)/(X2(n) - X1(n))^2; \tag{4.7}$$

This tells us the most accurate box which contains the disease i-e the patch enclosing the abnormal number of edges contains the disease.

In our example case :

$$\begin{aligned} \text{DBx} &= 15 \\ \text{Xstrt} &= 124 \\ \text{Xend} &= 186 \\ \text{Ystrt} &= 120 \\ \text{Yend} &= 182 \\ \text{Rat} &= 0.6948 \end{aligned}$$

bj =

Columns 1 through 9

0.6948 0.6938 0.6811 0.6709 0.7060 0.6763 0.6778 0.7021 0.7034

Columns 10 through 11

0.7151 0.6600

bg = 0.7151

where bj represents the ration of different patches and bg represents the patch having the max ratio i-e most accurate disease patch.

bww =

Columns 1 through 7

2671 2667 2618 2579 2714 2946 3321

Columns 8 through 11

2362 2051 2749 2537

bw = 3321

where bww represents array of max number of edges in each patch and bw is the patch containing maximum edges.

XstrtF = 130

XendF = 192

YstrtF = 126

YendF = 188

After determining the most precise coordinate points, these are applied to the original retinal image, and the respective area is cropped out of the RGB image. We take its histogram to determine where the red, green and blue components lie in the RGB color space. The image is converted into HSV color space and again its histogram is taken to determine the Hue, Saturation and Intensity component of the image.

For HE

Red	=	peaks at between 100-200 mostly at 150
Green	=	lies between 50-100
Blue	=	lies between 0 - 50
Hue	=	less 0.1
Saturation	=	$0.8 - 1$
Intensity	=	$0.5 - 0.8$

For CWS

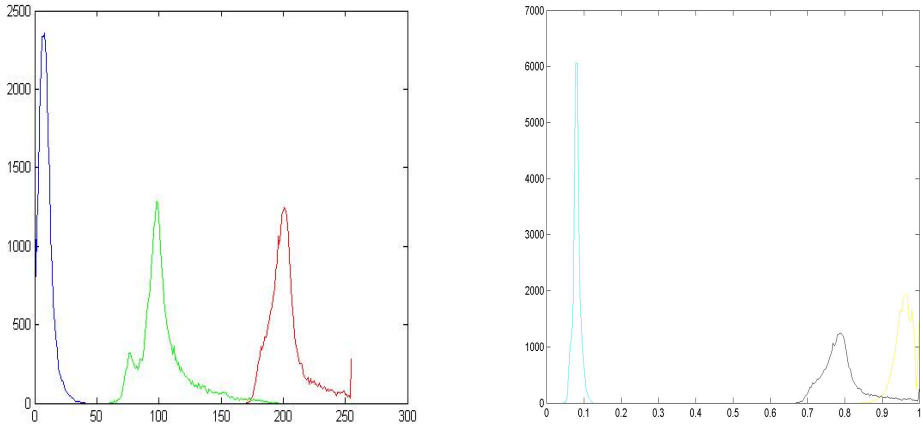

(a) (b)

Figure 4.2: HE disease a) RGB histogram, b) HSV histogram

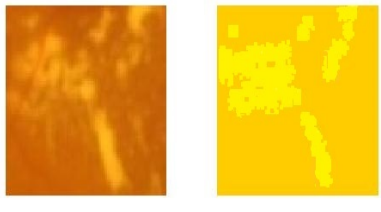

(a)

Figure 4.3: HE disease after applying color attributes

Red	=	peaks at between 200-250
Green	=	greater than 100
Blue	=	lies between 0-100
Hue	=	greater than 0.1
Saturation	=	$0.7 - 0.8$
Intensity	=	$0.8 - 1$

Few other examples of disease detection and their RGB and HSV graphs are shown in the following figures.

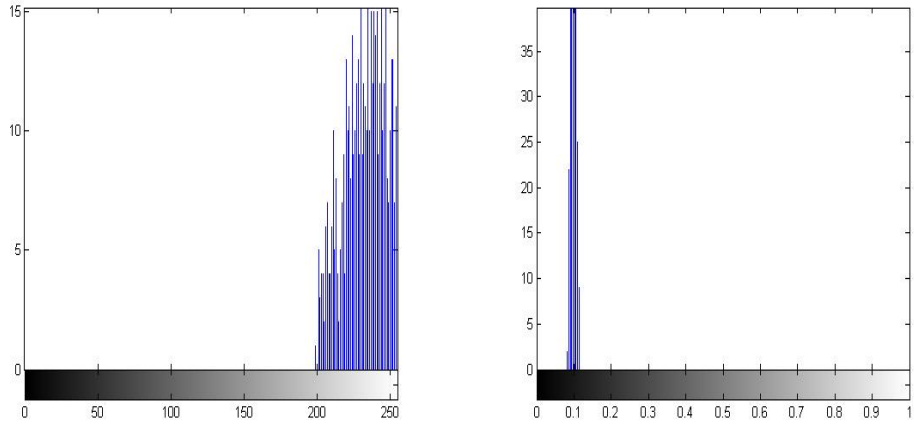

(a) (b)

Figure 4.4: a)Histogram of red component for HE disease after applying color attributes b)Histogram of hue component for HE disease after applying color attributes

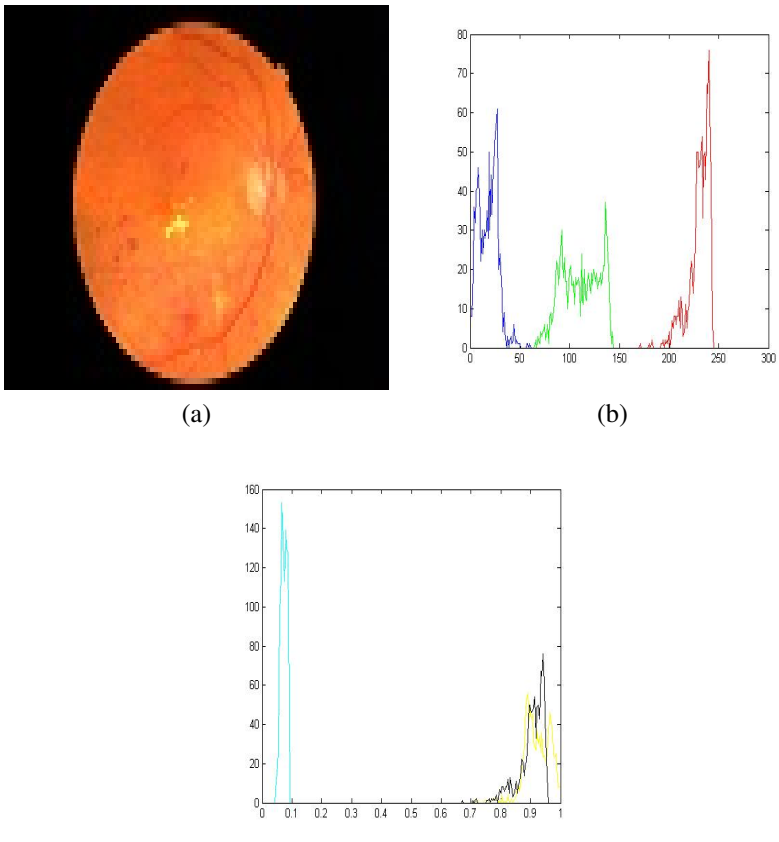

(a) (b)

(c)

Figure 4.5: CWS disease a) RGB histogram, b) HSV histogram

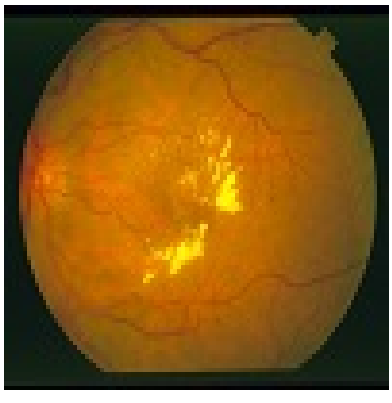

(a)

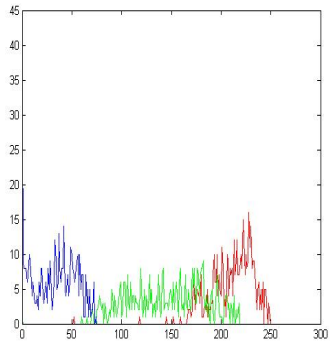

(b)

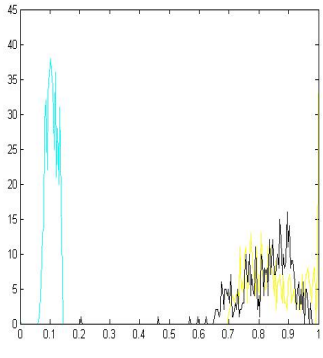

(c)

Figure 4.6: CWS disease a) RGB histogram, b) HSV histogram

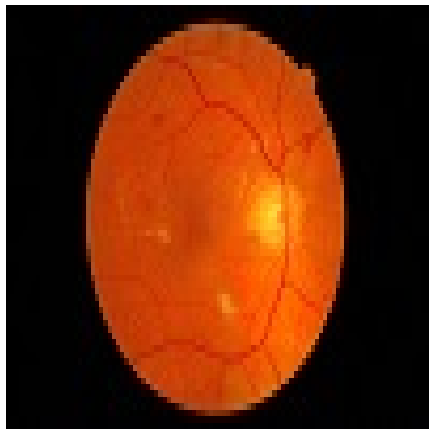

(a)

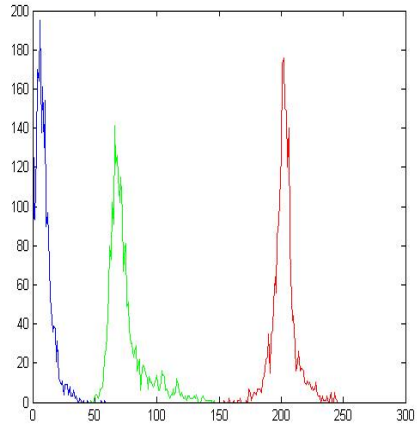

(b)

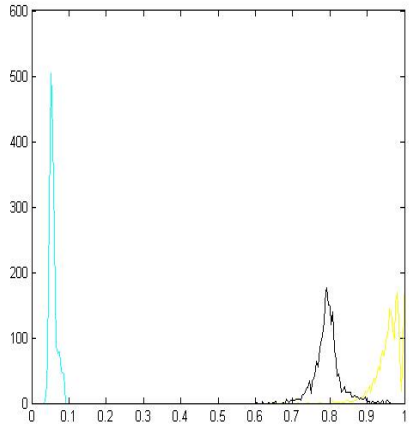

(c)

Figure 4.7: HE disease a) RGB histogram, b) HSV histogram

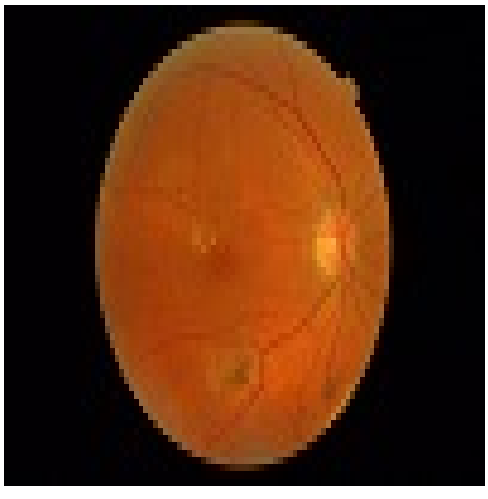

(a)

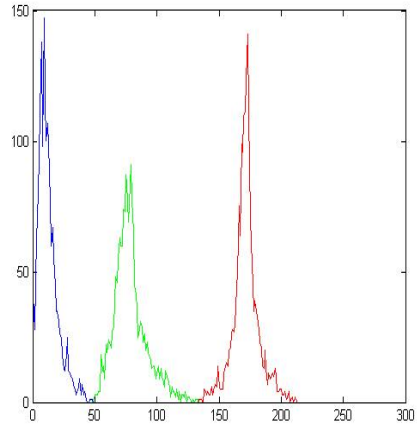

(b)

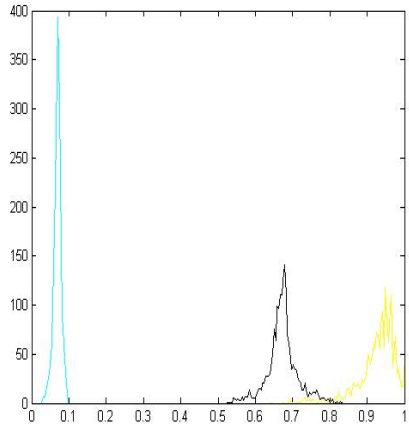

(c)

Figure 4.8: HE disease a) RGB histogram, b) HSV histogram

Chapter 5

CONCLUSION AND FUTURE WORK

5.1 Conclusion

Image processing has gained lot of importance over the last few years. Its applications are used in almost all the fields especially medical field. The growth of automated systems for detection of diabetic eye diseases is evolving with the exponential progression of information processing techniques and the development of cost-effective ophthalmic imaging devices. For practical applications all over the world numerous automated techniques are being designed. In the medical field many diseases are being pre-diagnosed with the help of advance systems and algorithms. Every year DR caused blindness accounts for twelve percent of all new cases of blindness, it is also the foremost reason of blindness in people belonging to age group 20 to 64. The chances of developing DR becomes higher the longer a person has diabetes. Most of the times diabetic retinopathy shows no early warning signs. A person with macular edema starts to have blurred vision, making everyday task like reading etc harder, it leads upto rapid loss of vision. Early signs of the disease can be retinal swelling, leaking blood vessels, damaged nerve tissue, fatty deposits on retina ,any changes in the blood vessels, new blood vessels etc. The proposed work will contribute to the development of a system which can be used in hospitals to pre-diagnose the cases and refer the relevant cases to the ophthalmologist attention since the manual work of retinal analysis is very time-consuming and influenced by human subjectivity so the automated disease detection can preprocess the relevant cases. Also this research will prove to be quite useful in many perspectives, such as help doctors in pre diagnosing the bright lesion cases in patients.

5.2 Future work

Retinal disease detection is a vast field, with many aspects on which more work can be done. For future works, the following can be recommend:

- Detection and classification of dark lesions.

- Detection and classification of non-proliferative diabetic retinopathy.
- Detection of other retinal diseases.
- Working on more features for disease detection like color, strength, texture, size, shape, edges, area and eccentricity.

BIBLIOGRAPHY

[1] E. Cummings, K. Facey, K. Macpherson, A. Morris, L. Reay, and J. Slattery, "Organisation of Services for Diabetic Retinopathy Screening," *Health Technology Assessment Report 1*, 2002.

[2] R. Fransen, T.L. Martin, W. Feuer, P. Hildebrand, Inoveon Health Research Group, "Clinical evaluation of patients with diabetic retinopathy: Accuracy of the Inoveon diabetic retinopathy-3DT system," *Ophthalmology*, vol 109, pp.595–601, 2002.

[3] A. Hansen, B. Sander, M. Larsen, J. Kleener, K.B. Johnsen, R. Klein, H.L. Andersen, "Screening for diabetic retinopathy using a digital non-mydriatic camera compared with standard 35-mm stereo colour transparencies," *Acta Ophthalmologica Scandinavica*, vol 82, pp. 656–665, 2004.

[4] B. Klein, R. Klein, P. McBride, K. Cruickshanks, M. Palta, M. Knudtson, J. Reinke, "Cardiovascular disease, mortality, and retinal microvascular characteristics in type 1 diabetes: Wisconsin epidemiologic study of diabetic retinopathy," *Archives of internal medicine*, vol 164, pp.1917–1924, 2004.

[5] R. van Leeuwen, U. Chakravarthy, J. Vingerling, C. Brussee, A. Hooghart, P. Mulder, P. Jong, "Grading of age-related maculopathy for epidemiological studies: is digital imaging as good as 35-mm film?," *Ophthalmology*, vol 110, pp.1540–1544, 2003.

[6] D.E. Singer, D.M. Nathan, H.A. Fogel, A.P. Schachat, "Screening for diabetic retinopathy," *Annals of Internal Medicine*, vol 116, pp.660–671, 1992.

[7] M.D. Abrmoff, K.G. Mona , M. Sonka, "Retinal imaging and image analysis," *Biomedical Engineering, IEEE Reviews*, vol 3, pp.169–208, 2010.

[8] M.D. Abrmoff, N. Meindert, M.S. Schulten, M. A. Viergever, S.R. Russell, B.V.Ginneken, "Evaluation of a system for automatic detection of diabetic retinopathy from color fundus photographs in a large population of patients with diabetes," *Diabetes care*, vol 31, pp.193–198, 2008.

[9] S. Philip, A.D. Fleming, K.A. Goatman, S. Fonseca, P. Mcnamee, G.S. Scotland, G.J. Prescott, P.F. Sharp, and J.A. Olson, "The efficacy of automated disease/no disease grading for diabetic retinopathy in a systematic screening programme," *British Journal of Ophthalmology*, vol 91, pp.152–1517, 2007.

[10] I. Liu, Y. Sun, "Recursive tracking of vascular networks in angiograms based on the detection-deletion scheme," *IEEE Transactions on Medical Imaging*, vol. 12, no. 2, pp. 334–341, 1993.

[11] H. Wang, W. Hsu, K. Goh, M. Lee, "An effective approach to detect lesions in color retinal images," *In Computer Vision and Pattern Recognition Proceedings in IEEE Conference*, vol 2, pp.181–186, 2000.

[12] L. Zhou, M.S. Rzeszotarski, L.J. Singerman, J.M. Chokreff, "The detection and quantification of retinopathy using digital angiograms," *IEEE Transactions on Medical Imaging*, vol. 13, no.4, pp.619-626, 1994.

[13] C. Heneghan, J. Flynn, M. O'Keefe, M. Cahill, "Characterization of changes in blood vessel and tortuosity in retinopathy of prematurity using image analysis," *Medical Image Analysis*, vol 6, pp.407-429, 2002.

[14] N. Patton, M.T. Aslam, T. MacGillivray, I.J. Deary, B. Dhillon, R.H. Eikelboom, K. Yogesan, I.J. Constable, "Retinal image analysis: concepts, applications and potential", *Progress in retinal and eye research*, vol 25, pp.99–127, 2006.

[15] O. Chutatape, L. Zheng, S.M. Krishnan, "Retinal blood vessel detection and tracking by matched Gaussian and Kalman filters," *Proceedings of the 20th Annual International Conference of the IEEE in Engineering in Medicine and Biology Society*, vol. 6, pp.3144-3149, 1998.

[16] Y.A. Tolias, S.M. Panas, "A fuzzy vessel tracking algorithm for retinal images based on fuzzy clustering," *IEEE Transactions on Medical Imaging*, vol. 17, no. 2, pp.263–273, 1998.

[17] F. Zana, J. Klein, "Segmentation of vessel-like patterns using mathematical morphology and curvature evaluation," *IEEE Transactions on Medical Imaging*, vol. 10, no. 7, pp.1010-1019, 2001.

[18] B. Fang, W. Hsu, M.L. Lee, "Reconstruction of vascular structures in retinal images," *Proceedings 2003 International Conference on Image Processing*, vol. 2, pp.157–160 , 2003.

[19] A.M. Mendonca, A. Campilho, "Segmentation of retinal blood vessels by combining the detection of centerlines and morphological reconstruction," *IEEE Transactions on Medical Imaging*, vol. 25, no. 9, pp. 1200–1213, 2006.

[20] A. Hoover, V. Kouznetsova, M. Goldbaum, "Locating blood vessels in retinal images by piecewise threshold probing of a matched filter response," *IEEE Transactions on Medical Imaging.*, vol. 19, no. 3, pp.203–210, 2000.

[21] L. Gang, O. Chutatape, S.M. Krishnan, "Detection and measurement of retinal vessels, in fundus images using amplitude modified second-order Gaussian filter," *IEEE Transactions on Biomedical Engineering*, vol. 49, no. 2, pp.168–172 , 2002.

[22] S. Chaudhuri, S. Chatterjee, N. Katz, M. Nelson, M. Goldbaum, "Detection of blood vessels in retinal images using two-dimensional matched filters," *IEEE Transactions on Medical Imaging*, vol. 8, no. 3, pp.263–269, 1989.

[23] M. Al-Rawi, M. Qutaishat, M. Arrar, "An improved matched filter for blood vessel detection of digital retinal images," *Computers in Biology and Medicine*, vol. 37, no. 2, pp.262–267, 2007.

[24] B. Al-Diri, A. Hunter, D. Steel, "An active contour model for segmenting and measuring retinal vessels," *IEEE Transactions on Medical Imaging*, vol. 28, no. 9, pp.1488-1497, 2009.

[25] M.E. Martinez-Prez, A.D. Hughes, S.A. Thom, A.A. Bharath, K.H. Parker, "Segmentation of blood vessels from red-free and fluorescein retinal images," *Medical Image Analysis*, vol. 11, no. 1, pp.47–61 , 2007.

[26] B. Lam, Y. Gao, A.C. Liew, "General retinal vessel segmentation using regularization-based multiconcavity modeling," *IEEE Transactions on Medical Imaging*, vol. 29, no. 7, pp.1369–1381, 2010.

[27] M. Niemeijer, J. Staal, B.V. Ginneken, M. Loog, M.D. Abramoff, "Comparative study of retinal vessel segmentation methods on a new publicly available database," *International Society for Optics and Photonics*, pp.648-656, 2004.

[28] J.B. Soares, J.G. Leandro, R.M. Cesar , H.F. Jelinek, M.J. Cree, "Retinal vessel segmentation using the 2-D Gabor wavelet and supervised classification," *IEEE Transactions on Medical Imaging*, vol. 25, no. 9, pp. 1214-1222, 2006.

[29] E. Ricci, R. Perfetti, "Retinal blood vessel segmentation using line operators and support vector classification," *IEEE Transactions on Medical Imaging*, vol. 26 , no. 10, pp.1357–1365 , 2007.

[30] D. Marin, A. Aquino, M. Gegundez-Arias and J.M. Bravo, A new supervised method for blood vessel segmentation in retinal images by using gray-level and moment invariants-based features," *IEEE Transactions on Medical Imaging*, vol. 30, no. 1, pp. 146–158, 2011.

[31] M. Fraz, P. Remagnino, A. Hoppe, B. Uyyanonvara, A. Rudnicka , C. Owen, S. Barman, " An ensemble classification-based approach applied to retinal blood vessel segmentation," *IEEE Transactions on Biomedical Engineering*, vol. 59 ,no. 9, pp.2538–2548, 2012.

[32] G. Azzopardi, N. Petkov, "A CORF computational model of a simple cell that relies on LGN input outperforms the Gabor function model," *Biological cybernetics*, vol. 106, no. 3, pp.177–189, 2012.

[33] G. Azzopardi, N. Petkov, "Automatic detection of vascular bifurcations in segmented retinal images using trainable COSFIRE filters," *Pattern Recognition Letters* , vol. 34, no. 8, pp. 922–933, 2013a.

[34] G. Azzopardi, N. Petkov, "Trainable COSFIRE filters for keypoint detection and pattern recognition," *IEEE Transactions on Pattern Analysis and Machine Intelligence*, vol. 35 , no. 2, pp.490–503, 2013b.

[35] G. Azzopardi, N. Strisciuglio, M. Vento and N. Petkov, Trainable COSFIRE filters for vessel delineation with application to retinal images, *Medical Image Analysis*, vol. 19, no. 1, pp.46–57, 2015.

[36] G. Azzopardi, N. Strisciuglio, M. Vento and N. Petkov, "Trainable COSFIRE filters for vessel delineation with application to retinal images," *Medical Image Analysis*, vol. 19, no. 1, pp.46–57, 2015.

[37] D. Mittal, V. kumar, S.C. Saxena, N. Khandelwal, Neural networks based focal liver diagnosis using ultrasound images, *Computerized Medical Imaging and Graphics*, vol 35, pp.135–323, 2011.

[38] K. Kumari, D. Mittal, Automated Drusen Detection Technique for Age-Related Macular Degeneration, *Journal of Biomedical Engineering and Medical Imaging*, vol 2, pp.19–26, 2015.

[39] R. Phillips, T. Spencer, P. Ross, P. Sharp, J. Forrester, Quantification of diabetic maculopathy by digital imaging of the fundus, *Eye*, vol. 5, pp.130-137, 1991.

[40] R. Phillips, J. Forrester, P. Sharp, Automated detection and quantification of retinal exudates, *Graefe's archive for clinical and experimental ophthalmology*, vol 231, pp.90-94, 1993.

[41] S. You, E. Bas, D. Erdogmus, J.kalpathy-Cramer, "Principal curve based retinal vessel segmentation towards diagnosis of retinal diseases," *IEEE International Conference on Healthcare Informatics, Imaging and Systems Biology*, pp.331337, 2011.

[42] G. Quellec, S.R. Russell, M.D. Abramoff, "Optimal Filter Framework for Automated, Instantaneous Detection of Lesions in Retinal Images," *Transactions on Medical Imaging* , vol. 30, no. 2, pp.523–233, 2011.

[43] K. Parasuraman, R. Ramya, "Automated detection of diseases by nicking quantification in retinal images," *International Conference on Electronics, Communication and Computational Engineering*, pp.331337, 2014.

[44] N.C. Mithun, S. Das, S.A. Fattah, "Automated detection of optic disc and blood vessel in retinal image using morphological, edge detection and feature extraction technique," *16th International Conference on Computer and Information Technology (ICCIT)* ,pp.98–102, 2014.

[45] A. McAndrew, "An introduction to digital image processing with matlab," *School of Computer Science and Mathematics, Victoria university of technology*, pp. 1-264, 2004.

[46] J.H. Hipwell, F. Strachan, J. Olson, K. McHard, P. Sharp, J. Forrester, "Automated detection of microaneurysms in digital red-free photographs: A diabetic retinopathy screening tool," *Diabetic medicine*, vol 17, pp.588–594, 2000.

[47] S. Pizer, E. Amburn, J. Austin, R. Cromartie, A. Geselowitz, T. Greer, B.T. Romeny, J. Zimmerman, K. Zuiderveld, "Adaptative histogram equalization and its varations," *Computer Visual Graphic Image Processing*, vol. 39, pp.355-368, 1987.

[48] M. Adzil, H. Nugroho, I. Iznita, "Contrast Enhancement of Retinal Vasculature in Digital Fundus Image," *International Conference on Digital Image Processing*, pp.137-141, 2009.

[49] A. Setiawan, T. Mengko, O. Santoso, A. Suksmono, "Color retinal image enhancement using CLAHE," *International Conference on ICT for Smart Society (ICISS)*, pp.1-3, 2013.

[50] J.V. Weijer, C. Schmid, J. Verbeek, D. Larlus, "Learning Color Names for Real-World Applications," *IEEE Transaction in Image Processing (TIP)*, pp.1512–1524, 2009.